# Heterogeneous & Homogeneous & Bio- & Nano-

# CHEM**CAT**CHEM

## CATALYSIS

## Accepted Article

**Title:** Robust In Situ Magnetic Resonance Imaging of Heterogeneous Catalytic Hydrogenation with and without Hyperpolarization

**Authors:** Kirill Viktorovich Kovtunov, Dmitry Lebedev, Alexandra Svyatova, Ekaterina V. Pokochueva, Igor P. Prosvirin, Evgeniy Y. Gerasimov, Valerii I. Bukhtiyarov, Christoph R. Müller, Alexey Fedorov, and Igor V. Koptyug

This manuscript has been accepted after peer review and appears as an Accepted Article online prior to editing, proofing, and formal publication of the final Version of Record (VoR). This work is currently citable by using the Digital Object Identifier (DOI) given below. The VoR will be published online in Early View as soon as possible and may be different to this Accepted Article as a result of editing. Readers should obtain the VoR from the journal website shown below when it is published to ensure accuracy of information. The authors are responsible for the content of this Accepted Article.

**To be cited as:** *ChemCatChem* 10.1002/cctc.201801820

**Link to VoR:** http://dx.doi.org/10.1002/cctc.201801820

A Journal of

ChemPubSoc
Europe

WILEY-VCH          www.chemcatchem.org

# COMMUNICATION

# Robust In Situ Magnetic Resonance Imaging of Heterogeneous Catalytic Hydrogenation with and without Hyperpolarization

Kirill V. Kovtunov,*[a,b] Dmitry Lebedev,[c] Alexandra Svyatova,[a,b] Ekaterina V. Pokochueva,[a,b] Igor P. Prosvirin,[d] Evgeniy Y. Gerasimov,[b, d] Valerii I. Bukhtiyarov,[d] Christoph R. Müller,[e] Alexey Fedorov,[e] and Igor V. Koptyug[a,b]

**Abstract:** Magnetic resonance imaging (MRI) is a powerful technique to characterize reactors during operating catalytic processes. However, MRI studies of heterogeneous catalytic reactions are particularly challenging because the low spin density of reacting and product fluids (for gas phase reactions) as well as magnetic field inhomogeneity, caused by the presence of a solid catalyst inside a reactor, exacerbate already low intrinsic sensitivity of this method. While hyperpolarization techniques such as parahydrogen induced polarization (PHIP) can substantially increase the NMR signal intensity, this general strategy to enable MR imaging of working heterogeneous catalysts to date remains underexplored. Here, we present a new type of model catalytic reactors for MRI that allow the characterization of a heterogeneous hydrogenation reaction aided by the PHIP signal enhancement, but also suitable for the imaging of regular non-polarized gases. These catalytic systems permit exploring the complex interplay between chemistry and fluid-dynamics that are typically encountered in practical systems, but mostly absent in simple batch reactors. High stability of the model reactors at catalytic conditions and their fabrication simplicity make this approach compelling for in situ studies of heterogeneous catalytic processes by MRI.

Catalytic processes (e.g., hydrogenation, reforming, oxidation, etc.) are at the cornerstone of chemical and petrochemical industry[1] and, to make these processes more sustainable, control over reaction selectivity, conversion rates, mass and heat transport inside the working reactor (that is under *operando* conditions) is required. Magnetic resonance imaging (MRI) is a tool applicable to operando studies that provide information for example about the distribution of liquids in the catalyst pellet during hydrogenation of α-methylstyrene[2] or heptene,[3] the coke profiles within a catalyst pellet,[4] the flow of water[5] or

propane[6] through a packed bed, the structure of a porous medium and the water flow during the deposition of fines,[7] or the velocities of particles in a fluidized bed.[8–10] MRI of reactors utilizing gases are not as developed as studies of liquids because the spin density in the gas phase is ca. 3 orders of magnitude lower relative to the condensed phase, which significantly limits the deployment of MRI for studying gases.[11] Nevertheless, a recent report showed that the distribution of the reactants and products inside a monolith type reactor can be measured even in the gas phase during ethylene hydrogenation reaction using two different catalyst supports, thereby revealing an effect of the support on the mass and heat transport.[12] Overall, to date, there are only a handful of MRI studies of the gas phase reactions with regular non-hyperpolarized gases.[13,14]

The limitation of low NMR sensitivity spurs the implementation of hyperpolarization techniques, which can potentially increase the intensity of NMR signals by up to several orders of magnitude, including spin-exchange optical pumping[15–17] (SEOP), dynamic nuclear polarization[18–20] (DNP) and parahydrogen-induced polarization[20–24] (PHIP) methods. SEOP relies on the polarization of noble gases, e.g., $^{129}Xe$,[25] $^{3}He$,[26] $^{83}Kr$[27], which are unreactive and very expensive. The necessity to use noble gases in SEOP narrows the scope of possible applications, in particular catalytic applications, but can provide information about gas mass transfer.[28] Other hyperpolarization methods are dissolution-DNP, a powerful tool to hyperpolarize small molecules in liquid solutions,[29,30] and DNP surface-enhanced NMR spectroscopy (DNP-SENS), which was used to study metal-organic frameworks and mesoporous materials.[31] However, DNP techniques require rather complex and very costly equipment[30] making studies exploiting these methods for polarization of gases limited to the preparation of small amounts of polarized propane, butane and ethylene using HYPSOs (Hyper Polarizing Solids).[32] Taking into account mentioned constrains of the polarizable gases in SEOP and DNP methods, heterogeneous PHIP[33,34] (HET-PHIP) has emerged as an attractive alternative because of its simplicity and robustness for the production of hyperpolarized (HP) gases. This method is based on the pairwise addition of parahydrogen (p-$H_2$) instead of normal hydrogen (hydrogen at thermal equilibrium, n-$H_2$) in a hydrogenation reaction, i.e. when two hydrogen atoms from the same $H_2$ molecule are added to the same substrate molecule with breaking of magnetic symmetry, leading to the overpopulation of spin states and consequently to hyperpolarization.[35]

The PHIP phenomenon was observed in homogeneous[36] and heterogeneous catalysis.[37] With homogeneous catalysts, there is a general problem of catalyst separation from the hyperpolarized product, although they still can be used for the production of HP gases[38,39], small molecules,[40,41] including bioactive ones,[42–44] and examination of reactive

[a] Dr. K. V. Kovtunov, A. Svyatova, E.V. Pokochueva, Prof. I. V. Koptyug, International Tomography Center, SB RAS
3A Institutskaya st., Novosibirsk 630090, Russia
E-mail: kovtunov@tomo.nsc.ru

[b] Dr. K. V. Kovtunov, Dr. Evgeniy Y. Gerasimov, A. Svyatova, E.V. Pokochueva, Prof. I. V. Koptyug, Novosibirsk State University
2 Pirogova st., Novosibirsk 630090, Russia

[c] Dr. D. Lebedev, ETH Zürich, Department of Chemistry and Applied Biosciences, Vladimir-Prelog-Weg 1-5, CH 8093, Zürich, Switzerland

[d] Dr. I. P. Prosvirin, Dr. E. Y. Gerasimov, Prof. V. I. Bukhtiyarov, Boreskov Institute of Catalysis, SB RAS
5 Acad. Lavrentiev pr., Novosibirsk 630090, Russia

[e] Dr. A. Fedorov, Prof. C. R. Müller, ETH Zürich, Department of Mechanical and Process Engineering, Leonhardstrasse 21, CH 8092 Zürich, Switzerland

intermediates.[45] On the other hand, heterogeneous catalysts have the advantage of easy separation and recycling,[46] which is particularly important for biomedical applications and studies of catalytic reactors.[47–49] Several imaging reports of HP products relied on the PHIP methodology with conventional MRI scanners,[50–53] however, only two studies have used PHIP for imaging of the formed hyperpolarized gas within a catalyst bed directly[54] and by applying remote detection NMR technique.[55] This can be explained by the low spin density of gases compared to liquids, inhomogeneity of the magnetic field inside reactors caused by solid catalyst beads[6,8,56] and the fast diffusion of gases.[57–59] All of these factors decrease the signal intensity significantly. Raising the pressure in the system does increase the gas density and, consequently, the signal intensity, however, most reactors suitable for MRI studies are non-metallic and therefore limited to low pressure processes. That said, a custom-built cylindrical reactor made of silicon nitride ($Si_3N_4$) was implemented for the study of ethene oligomerization at 28 barg; the products were expected to be in a liquid phase under these conditions.[60] The reactor contained pellets of $Ni/SiO_2-Al_2O_3$ catalyst and, despite the pronounced line broadening in the NMR spectra, the total conversion rates and distribution of products were determined in operando mode. However, no information on spatial distribution of the products within the catalyst bed was reported, and susceptibility broadening made direct identification of products from the NMR spectra very difficult.

Here, we present the fabrication of model glass reactors with catalytic coatings compatible with operando MRI studies that minimize the perturbation of the magnetic field homogeneity and thereby do not decrease the NMR signal intensity of the reactants and products. In particular, we have performed MR imaging of the catalytic propene hydrogenation using Rh nanoparticles supported on the $TiO_2$ layer deposited on glass reactors with arbitrary patterns of the $Rh/TiO_2$ catalyst as described in detail below.

We have started our studies by optimizing loadings of the active metal (Rh) to maximize signal enhancement in propene hydrogenation with parahydrogen (p-$H_2$) using custom-made glass reactors in PASADENA conditions, i.e. in a high magnetic field of the NMR spectrometer. Our reactor fabrication procedure introduces the active phase by impregnation of a molecular rhodium precursor (chloro(1,5-cyclooctadiene)rhodium(I) dimer) onto arbitrarily selected areas of tailor-shaped glass reactors covered with a thin porous layer of $TiO_2$. This 8 μm thick layer of porous oxide support (Figure 1a) was prepared by the dip-coating of a 10 mm height, 5 mm outer diameter borosilicate glass tube with a $TiO_2$ paste (see Supporting information for detailed procedure). An in situ reductive treatment of impregnated reactors (1.5 mL s$^{-1}$ H$_2$ flow, 130 °C, 1 hour) yields catalytically active porous $Rh/TiO_2$ coatings (Figure 1b and 1d). Reactors of cylindrical tubes and rectangular plates (Figures S1-S2) with a thin layer of titania were chosen to provide efficient heat and mass transfer conditions, rendering kinetics of studied catalytic process close to intrinsic. These two factors in combination with the high mechanical stability and only a minor perturbation of the magnetic field homogeneity by our reactors

are beneficial for studies of catalytic hydrogenation reactions by MRI. A representative reactor tube with a reactive $Rh/TiO_2$ coating is shown in Figure 1c, other studied reactors are shown in Figures S1-S2.
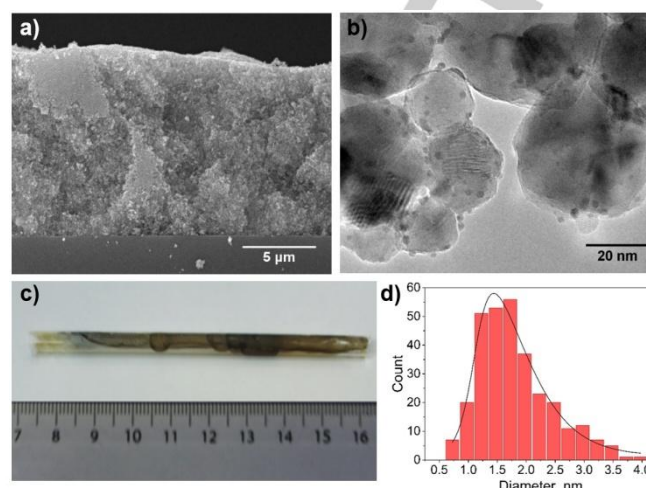


**Figure 1.** (a) SEM image of the glass-catalyst interface; (b) TEM image of Rh particles distributed on $TiO_2$ support for the spent catalyst; (c) representative image of the cylindrical glass reactor tube used for the MRI hydrogenation studies with a Rh active phase that was arbitrarily introduced to one side of the tube; (d) histogram of the particle size distribution obtained from TEM images of the spent catalyst.

All tested reactors were catalytically active in hydrogenation of propene at room temperature, revealing enhanced ^{1}H NMR signals of propane due to the pairwise addition of hydrogen; glass plates featured a similar activity as glass tubes (Figures S3-S4). A tube with the highest enhancement of propane NMR signals contained ca. 0.7 μmol of Rh arbitrarily covering ca. two thirds of the tube surface (Figure 1c) and was selected for optimizing the flow rate of the propene-hydrogen gas mixture (1:3.5 ratio) to identify conditions for the highest proton NMR signal enhancement. Experiments with normal hydrogen (statistical mixture of ortho- and para- isomers, n-$H_2$) showed that conversion increases at low flow rates due to longer contact times (Figure S5). On the other hand, hydrogenation with p-$H_2$ requires relatively high gas flow rates in order to minimize the overlap of hyperpolarized and thermal NMR signals of the product and to decrease the influence of relaxation processes on the decay of the hyperpolarized NMR signal.[51] Indeed, at 1.8 mL s$^{-1}$ flow rate of the reactant gases there are no detectable propane signals with the characteristic antiphase shapes associated with the PHIP effect (Figure 2). However, increasing the flow rate already to 3.6 mL s$^{-1}$ leads to the hyperpolarized propane peaks that are further enhanced at 8.8 mL s$^{-1}$ (Figure 2).
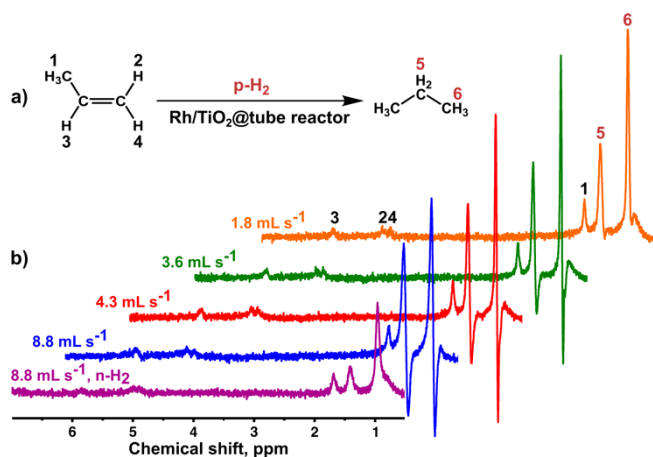
**Figure 2.** a) Hydrogenation of propene with p-$H_2$, b) $^1$H NMR spectra acquired during the room temperature hydrogenation of propene with p-$H_2$ at different gas flow rates (ranging from 1.8 to 8.8 mL s$^{-1}$) as well as an $^1$H NMR spectrum acquired with n-$H_2$ using 8.8 mL s$^{-1}$ gas flow rate.

Notably, the performance of the catalytic reactor in Figure 1c was stable even after 9 days of use, the observed signal enhancement at the end of this time was ca. 3-fold (Figure S6). The X-ray photoelectron spectroscopy (XPS) data recorded from the catalytic coating after 9 days of use showed that the rhodium phase on titania was metallic Rh(0) (Figure S7). A slight decrease of NMR signal enhancement (but not conversion) relative to the fresh sample can be explained by the blocking of the pairwise hydrogen addition centers by formed carbon depositions, consistent with the XPS analysis showing a high carbon content.[61] The average diameter of Rh(0) nanoparticles from the spent sample was 1.5-2 nm (Figure 1b,d).

With the optimized conditions for propene hydrogenation in hand, MRI studies of the working catalytic reactor during propene hydrogenation were performed using a conventional fast low angle shot (FLASH)[62] pulse sequence for imaging in pseudo-3D mode, i.e. the stack of acquired 2D slices was transformed to a 3D image (Figure 3). A catalytic reactor with 5 mm o.d. was placed inside a 10 mm standard NMR tube and 1/16" Teflon capillary was passed to the bottom of the NMR tube through the reactor. Since the catalytic coating is thereby positioned on the outside walls of the 5 mm glass reactor, the hydrogenation reaction proceeds in the space between the 5 mm and 10 mm tubes (dashed red and solid black lines in Figure 3, respectively). Moreover, due to the arbitrary non-uniform pattern of areas with deposited rhodium (Figure 1a) the reaction could take place only on these Rh-containing parts of the reactor, which was validated via MR imaging of the formed hydrogenation product (propane). Detection of MR images in a short period of time with FLASH allowed recording 2D $^1$H MR images of propane within 3 minutes 52 seconds (8 slices of 10 mm thickness, repetition time (TR) 113.6 ms) with a high spatial resolution of 0.125×0.125 cm$^2$/pixel and signal-to-noise ratio (SNR) of 15 and 33 for n-$H_2$ and p-$H_2$, respectively. Importantly, FLASH sequence[63] enabled separation of maximal contributions from thermally polarized signals (conventional shape of $^1$H NMR signals) and hyperpolarized signals (antiphase,

PASADENA shape signals) by varying the echo time (TE) of the pulse sequence.[36] Echo times of 10 ms and 8 ms provide the highest SNR during in situ MRI visualization of heterogeneous hydrogenation of propene to propane with n-$H_2$ and p-$H_2$, respectively (Figure S8).
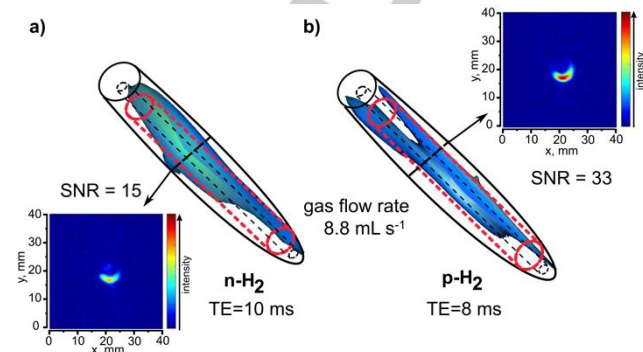


**Figure 3.** 3D model of the gas flow containing mixture of a) propene:n-$H_2$ and b) propene:p-$H_2$ at 1:3.5 ratio at the flow rate of 8.8 mL s$^{-1}$. The black solid line shows the edges of the NMR tube, the red dashed line corresponds to the reactor glass tube, the black dashed line corresponds to the Teflon capillary. Slice thickness was 10 mm with 5 mm interslice distance between centers of slices, number of slices was 8, number of averages was 64. Color bar corresponds to signal intensity.

MRI results presented in Figure 3 demonstrate two possible imaging applications. Firstly, the 3D geometry of our working catalytic reactors can be visualized by imaging of the formed thermally polarized propane in hydrogenation with n-$H_2$ (Figure 3a). Secondly, the catalytically active region of the model tube reactor can be selectively imaged during hydrogenation with p-$H_2$ due to the instantaneous formation of hyperpolarized propane onto catalytically active areas (Figure 3b). Therefore, an indirect method of a 3D visualization of the catalytically active layer during heterogeneous hydrogenation was enabled for the first time by MRI. Note that by varying TE we can detect only the formed hyperpolarized propane gas[36,50] and no signals from the thermally polarized reactants were detected. Short TE allows observing the MR image of the thermally produced propane when hydrogenation is carried out with normal hydrogen (Figure S8). Therefore, having sufficient SNR even with n-$H_2$, we performed additional experiments by varying the flow rate. Despite the fact that it took significantly longer time to obtain the same spatial resolution as in the experiments with p-$H_2$ (ca. 31 minutes vs. 4 minutes), the experiment with n-$H_2$ indeed allowed collecting MR images even with the use of normal $H_2$, showing the feasibility of using our reactors for operando characterization of chemical reactions without hyperpolarization (Figure 4).
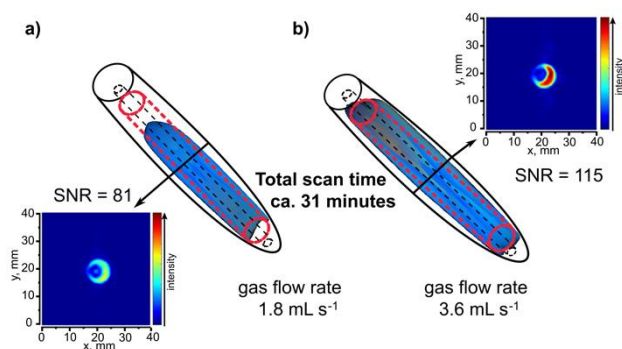
**Figure 4.** 3D model of the gas flow containing mixture of propene:n-$H_2$ = 1:3.5 at the flow rate a) 1.8 and b) 3.6 mL s$^{-1}$. Slice thickness was 5 mm with 1 mm interslice distance, number of slices was 16, number of averages was 256. Notations are the same as in Figure 3.

Although a premixing of the signal from the unreacted propene to the formed propane signal slightly distorts the resulting MR images, our results demonstrate that the catalytically active region and geometry of the reactor can be visualized by conventional $^1$H MRI. In all MRI experiments, we achieved a slightly better spatial resolution (0.125×0.125 cm$^2$/pixel) compared to the current state-of-the-art studies where spatial resolution of 0.15×0.15 cm$^2$/pixel was obtained.[14]

In conclusion, we have reported a robust method for MR imaging of catalytic hydrogenation processes utilizing parahydrogen-induced polarization. PHIP is one of the most convenient techniques of exploiting signal enhancement by polarization that combines setup simplicity and suitability for studying gas phase products of catalytic hydrogenation reactions, avoiding the problem of low spin density that leads to low signal intensity. In order to prevent distortion of field homogeneity by catalysts beads we have developed a novel type of MRI compatible reactors featuring Rh nanoparticles supported on a porous TiO$_2$ layer deposited on glass tubes or plates. Such catalyst design demonstrates a high mechanical stability coupled with minimized heat and mass transfer limitations due to the thin TiO$_2$ layer on the glass surface. More importantly, this catalyst design is able to implement pairwise hydrogen addition routes opening the door to the deployment of PHIP-based MRI strategies. MRI experiments conducted utilizing a conventional FLASH pulse sequence in a pseudo-3D mode with optimized parahydrogen propene hydrogenation conditions and pulse sequence parameters allowed obtaining the 2D images of a working glass tube reactor with a catalytic Rh/TiO$_2$ coating with a spatial resolution of 0.125×0.125 cm$^2$/pixel and transforming them into a 3D data set. Our approach is suitable for fast image acquisition as the total scan time was only ca. 4 minutes. It should be noted that the method itself can be extended to the use of normal hydrogen as well, with the signal-to-noise ratio of ca. 100 when the total scan time was extended to ca. 30 minutes, sufficient for obtaining images with the aforementioned spatial resolution.

## Experimental Section

Glass tube reactors were prepared by deposition of a paste containing TiO$_2$ and organic binder (hydroxypropyl cellulose) on the outer surface of 5 mm glass tubes using dip-coating method with the subsequent calcination in air at 500 °C. Deposition of Rh was performed with a micropipette using a solution of [(COD)RhCl]$_2$ in acetonitrile (see SI for details). All reactors were activated in the flow of hydrogen (1.5 mL s$^{-1}$) at 130 °C for 1 hour and then cooled down without termination of the H$_2$ flow. Commercially available propene and hydrogen were used as received. For PHIP experiments, hydrogen gas was enriched with parahydrogen up to ~90% using Bruker parahydrogen generator BPHG 90. Glass reactor tube was placed at the bottom of a 10 mm NMR tube, and the gas mixture was supplied through a 1/16" OD PTFE capillary. Hydrogenation was performed in a 9.4 T field of the NMR spectrometer at atmospheric pressure and room temperature. The gas flow rate was varied from 1.8 to 8.8 mL s$^{-1}$ using an Aalborg rotameter. NMR and MRI experiments were performed on a Bruker Avance III 400 MHz NMR spectrometer equipped with microimaging accessories. The experiments were conducted with a commercial 15 mm ID RF coil utilizing $^1$H channel. $^1$H NMR spectra were acquired using a single π/4 pulse. $^1$H MRI of 10 mm NMR tube containing the glass tube was done utilizing FLASH pulse sequence with a 30 degree flip angle. In the experiments, matrix size was 32 x 32, which was zero-filled to 128 x 128. Spatial resolution was 0.125 x 0.125 cm$^2$/pixel. For the experiments with normal hydrogen and flow rate variation, 16 slices of 5 mm thickness and 1 mm interslice distance between centers of slices were imaged, number of averages was 256. Echo time was 10 ms, total scan time was 31 minutes. For the experiments with comparison of thermal and hyperpolarized gas, number of slices was 8, slice thickness was 10 mm with 5 mm interslice distance between centers of slices. Number of averages was 64. Echo time was 10 ms in case of thermal gas and 8 ms in case of hyperpolarized gas, total scan time was 3 minutes 52 seconds. 3D data sets were reconstructed using ImageJ software from stack of slices obtained by MRI.

## Acknowledgements

## References

[1]     R. Schlögl, *Angew. Chemie Int. Ed.* **2015**, *54*, 3465–3520.
[2]     I. V. Koptyug, A. A. Lysova, A. V. Kulikov, V. A. Kirillov, V. N. Parmon, R. Z. Sagdeev, *Appl. Catal. A Gen.* **2004**, *267*, 143–148.
[3]     V. A. Kirillov, I. V. Koptyug, *Ind. Eng. Chem. Res.* **2005**, *44*, 9727–9738.
[4]     K. Y. Cheah, N. Chiaranussati, M. P. Hollewand, L. F. Gladden, *Appl. Catal. A, Gen.* **1994**, *115*, 147–155.
[5]     I. V. Koptyug, A. A. Lysova, A. V. Matveev, V. N. Parmon, R. Z. Sagdeev, *Top. Catal.* **2005**, *32*, 83–91.
[6]     I. V. Koptyug, A. A. Lysova, A. V. Matveev, L. Y. Ilyina, R. Z.

Sagdeev, V. N. Parmon, *Magn. Reson. Imaging* **2003**, *21*, 337–343.

[7] A. J. Sederman, L. F. Gladden, *Magn. Reson. Imaging* **2001**, *19*, 565–567.

[8] C. R. Muller, D. J. Holland, A. J. Sederman, M. D. Mantle, L. F. Gladden, J. F. Davidson, *Powder Technol.* **2008**, *183*, 53–62.

[9] I. V. Koptyug, A. V. Khomichev, A. A. Lysova, R. Z. Sagdeev, *J. Am. Chem. Soc.* **2008**, *130*, 10452–10453.

[10] A. A. Lysova, A. V. Kulikov, V. N. Parmon, R. Z. Sagdeev, I. V. Koptyug, *Chem. Commun.* **2012**, *48*, 5763.

[11] V. V. Zhivonitko, A. I. Svyatova, K. V. Kovtunov, I. V. Koptyug, *Recent MRI Studies on Heterogeneous Catalysis*, Academic Press, **2018**.

[12] J. Ulpts, W. Dreher, L. Kiewidt, M. Schubert, J. Thöming, *Catal. Today* **2016**, *273*, 91–98.

[13] J. Ulpts, L. Kiewidt, W. Dreher, J. Thöming, *Catal. Today* **2018**, *310*, 176–186.

[14] J. Ulpts, W. Dreher, M. Klink, J. Thöming, *Appl. Catal. A Gen.* **2015**, *502*, 340–349.

[15] T. G. Walker, W. Happer, *Rev. Mod. Phys.* **1997**, *69*, 629–642.

[16] D. M. L. Lilburn, G. E. Pavlovskaya, T. Meersmann, *J. Magn. Reson.* **2013**, *229*, 173–186.

[17] B. M. Goodson, *J. Magn. Reson.* **2002**, *155*, 157–216.

[18] T. Maly, G. T. Debelouchina, V. S. Bajaj, K.-N. Hu, C.-G. Joo, M. L. Mak–Jurkauskas, J. R. Sirigiri, P. C. A. van der Wel, J. Herzfeld, R. J. Temkin, et al., *J. Chem. Phys.* **2008**, *128*, 052211.

[19] U. L. Günther, in *Clin. Exp. Rheumatol.*, **2011**, pp. 23–69.

[20] J. Van Bentum, B. Van Meerten, M. Sharma, A. Kentgens, *J. Magn. Reson.* **2016**, *264*, 59–67.

[21] C. R. Bowers, D. P. Weitekamp, *J. Am. Chem. Soc.* **1987**, *109*, 5541–5542.

[22] M. G. Pravica, D. P. Weitekamp, *Chem. Phys. Lett.* **1988**, *145*, 255–258.

[23] R. A. Green, R. W. Adams, S. B. Duckett, R. E. Mewis, D. C. Williamson, G. G. R. Green, *Prog. Nucl. Magn. Reson. Spectrosc.* **2012**, *67*, 1–48.

[24] J. Bargon, R. Giernoth, L. Greiner, L. Kuhn, S. Laue, *In Situ NMR Methods in Catalysis*, Springer, Heidelberg, **2007**.

[25] L. Schröder, *Phys. Medica* **2013**, *29*, 3–16.

[26] A. Ben-Amar Baranga, S. Appelt, M. V. Romalis, C. J. Erickson, A. R. Young, G. D. Cates, W. Happer, *Phys. Rev. Lett.* **1998**, *80*, 2801–2804.

[27] Z. I. Cleveland, G. E. Pavlovskaya, N. D. Elkins, K. F. Stupic, J. E. Repine, T. Meersmann, *J. Magn. Reson.* **2008**, *195*, 232–237.

[28] G. Pavlovskaya, J. Six, T. Meersman, N. Gopinathan, S. P. Rigby, *AIChE J.* **2015**, *61*, 4013–4019.

[29] J. H. Ardenkjaer-Larsen, B. Fridlund, A. Gram, G. Hansson, L. Hansson, M. H. M. H. Lerche, R. Servin, M. Thaning, K. Golman, *Proc. Natl. Acad. Sci. U. S. A.* **2003**, *100*, 10158–10163.

[30] M. S. Albert, F. T. Hane, Eds. , *Hyperpolarized and Inert Gas MRI: From Technology to Application in Research and Medicine*, Academic Press, **2017**.

[31] A. J. Rossini, A. Zagdoun, M. Lelli, A. Lesage, C. Copéret, L. Emsley, *Acc. Chem. Res.* **2013**, *46*, 1942–1951.

[32] B. Vuichoud, E. Canet, J. Milani, A. Bornet, D. Baudouin, L. Veyre, D. Gajan, L. Emsley, A. Lesage, C. Copéret, et al., *J. Phys. Chem. Lett.* **2016**, *7*, 3235–3239.

[33] I. V Koptyug, K. V Kovtunov, S. R. Burt, M. Sabieh Anwar, C. Hilty, S.-I. Han, A. Pines, R. Z. Sagdeev, *J. Am. Chem. Soc.* **2007**, *129*, 5580–5586.

[34] K. V. Kovtunov, V. V. Zhivonitko, I. V. Skovpin, D. A. Barskiy, I. V. Koptyug, *Top. Curr. Chem.* **2013**, *338*, 123–180.

[35] T. C. Eisenschmid, R. U. Kirss, P. P. Deutsch, S. I. Hommeltoft, R. Eisenberg, J. Bargon, R. G. Lawler, A. L. Balch, *J. Am. Chem. Soc.* **1987**, *109*, 8089–8091.

[36] L. Buljubasich, M. B. Franzoni, K. Münnemann, *Top. Curr. Chem.* **2013**, *338*, 33–74.

[37] K. V. Kovtunov, D. A. Barskiy, A. M. Coffey, M. L. Truong, O. G. Salnikov, A. K. Khudorozhkov, E. A. Inozemtseva, I. P. Prosvirin, V.

I. Bukhtiyarov, K. W. Waddell, et al., *Chem. Eur. J.* **2014**, *20*, 11636–11639.

[38] K. V. Kovtunov, D. A. Barskiy, R. V. Shchepin, A. M. Coffey, K. W. Waddell, I. V. Koptyug, E. Y. Chekmenev, *Anal. Chem.* **2014**, *86*, 6192–6196.

[39] K. V Kovtunov, V. V. Zhivonitko, I. V. Skovpin, D. A. Barskiy, O. G. Salnikov, I. V. Koptyug, *J. Phys. Chem. C* **2013**, *117*, 22887–22893.

[40] T. Jonischkeit, U. Bommerich, J. Stadler, K. Woelk, H. G. Niessen, J. Bargon, *J. Chem. Phys.* **2006**, *124*, 201109.

[41] M. Roth, P. Kindervater, H. P. Raich, J. Bargon, H. W. Spiess, K. Münnemann, *Angew. Chemie - Int. Ed.* **2010**, *49*, 8358–8362.

[42] M. Körner, G. Sauer, A. Heil, D. Nasu, M. Empting, D. Tietze, S. Voigt, H. Weidler, T. Gutmann, O. Avrutina, et al., *Chem. Commun.* **2013**, *49*, 7839–7841.

[43] G. Sauer, D. Nasu, D. Tietze, T. Gutmann, S. Englert, O. Avrutina, H. Kolmar, G. Buntkowsky, *Angew. Chemie - Int. Ed.* **2014**, *53*, 12941–12945.

[44] J. B. Hövener, A. N. Pravdivtsev, B. Kidd, C. R. Bowers, S. Glöggler, K. V Kovtunov, M. Plaumann, R. Katz-Brull, K. Buckenmaier, A. Jerschow, et al., *Angew. Chemie - Int. Ed.* **2018**, *57*, 11140–11162.

[45] A. S. Kiryutin, G. Sauer, A. V. Yurkovskaya, H. H. Limbach, K. L. Ivanov, G. Buntkowsky, *J. Phys. Chem. C* **2017**, *121*, 9879–9888.

[46] L. S. Bouchard, K. V. Kovtunov, S. R. Burt, S. Anwar, I. V. Koptyug, R. Z. Sagdeev, A. Pines, *Angew. Chemie - Int. Ed.* **2007**, *46*, 4064–4068.

[47] J. McCormick, S. Korchak, S. Mamone, Y. N. Ertas, Z. Liu, L. Verlinsky, S. Wagner, S. Glöggler, L. S. Bouchard, *Angew. Chemie - Int. Ed.* **2018**, *57*, 10692–10696.

[48] S. Glöggler, A. M. Grunfeld, Y. N. Ertas, J. McCormick, S. Wagner, P. P. M. Schleker, L. Bouchard, *Angew. Chemie Int. Ed.* **2015**, *54*, 2452–2456.

[49] S. Glöggler, J. Colell, S. Appelt, *J. Magn. Reson.* **2013**, *235*, 130–142.

[50] K. V. Kovtunov, A. S. Romanov, O. G. Salnikov, D. A. Barskiy, E. Y. Chekmenev, I. V. Koptyug, *Tomography* **2016**, *2*, 49–55.

[51] D. B. Burueva, A. S. Romanov, O. G. Salnikov, V. V. Zhivonitko, Y.-W. W. Chen, D. A. Barskiy, E. Y. Chekmenev, D. W. Hwang, K. V. Kovtunov, I. V. Koptyug, *J. Phys. Chem. C* **2017**, *121*, 4481–4487.

[52] D. B. Burueva, K. V. Kovtunov, A. V. Bukhtiyarov, D. A. Barskiy, I. P. Prosvirin, I. S. Mashkovsky, G. N. Baeva, V. I. Bukhtiyarov, A. Y. Stakheev, I. V. Koptyug, *Chem. Eur. J.* **2018**, *24*, 2547–2553.

[53] K. V. Kovtunov, M. L. Truong, D. A. Barskiy, I. V. Koptyug, A. M. Coffey, K. W. Waddell, E. Y. Chekmenev, *Chem. Eur. J.* **2014**, *20*, 14629–14632.

[54] L.-S. S. Bouchard, S. R. Burt, M. S. Anwar, K. V. Kovtunov, I. V. Koptyug, A. Pines, *Science* **2008**, *319*, 442–445.

[55] V. V. Zhivonitko, V. V. Telkki, I. V. Koptyug, *Angew. Chemie - Int. Ed.* **2012**, *51*, 8054–8058.

[56] L. F. Gladden, F. J. R. Abegão, C. P. Dunckley, D. J. Holland, M. H. Sankey, A. J. Sederman, *Catal. Today* **2010**, *155*, 157–163.

[57] L. F. Gladden, *Top.Catal.* **2003**, *24*, 19–28.

[58] J.-G. Choi, D. D. Do, H. D. Do, *Ind. Eng. Chem. Res.* **2001**, *40*, 4005–4031.

[59] P. Stevenson, A. J. Sederman, M. D. Mantle, X. Li, L. F. Gladden, *J. Colloid Interface Sci.* **2010**, *352*, 114–120.

[60] S. T. Roberts, M. P. Renshaw, M. Lutecki, J. McGregor, A. J. Sederman, M. D. Mantle, L. F. Gladden, *Chem. Commun.* **2013**, *49*, 10519–10521.

[61] K. V. Kovtunov, D. A. Barskiy, O. G. Salnikov, A. K. Khudorozhkov, V. I. Bukhtiyarov, I. P. Prosvirin, I. V. Koptyug, *Chem. Commun.* **2014**, *50*, 875–878.

[62] A. Haase, J. Frahm, D. Matthaei, W. Hanicke, K. D. Merboldt, *J. Magn. Reson.* **1986**, *67*, 258–266.

[63] K. V. Kovtunov, B. E. Kidd, O. G. Salnikov, L. B. Bales, M. E. Gemeinhardt, J. Gesiorski, R. V. Shchepin, E. Y. Chekmenev, B. M. Goodson, I. V. Koptyug, *J. Phys. Chem. C* **2017**, *121*, 25994–25999.

## COMMUNICATION

# COMMUNICATION

Conventional MRI technique was successfully used for the imaging of a heterogeneous hydrogenation of propene to propane with and without hyperpolarization. A new type of model reactors with a coating of the active Rh/TiO$_2$ layer was developed for imaging applications of working catalytic reactors by MRI. The arbitrarily introduced areas containing the active phase were successfully identified by the formed gas with high spatial resolution.
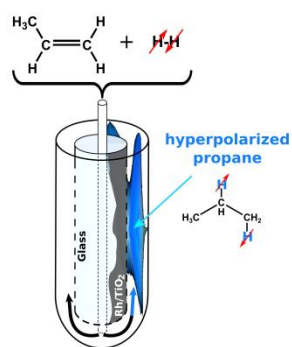
*Kirill V. Kovtunov\*, Dmitry Lebedev, Alexandra Svyatova, Ekaterina V, Pokochueva, Igor P. Prosvirin, Evgeniy Y. Gerasimov, Valerii I. Bukhtiyarov, Cristoph R. Müller, Alexey Fedorov, and Igor V. Koptyug*

***Page No. – Page No.***

**Robust In Situ Magnetic Resonance Imaging of Heterogeneous Catalytic Hydrogenation with and without hyperpolarization**